

# Assessment of Near-field Pollutant Dispersion: Effect of Upstream Buildings

M. Chavez <sup>a\*</sup>, B. Hajra <sup>a</sup>, T. Stathopoulos <sup>a</sup>, A. Bahloul <sup>b</sup>

<sup>a</sup>Department of Building, Civil and Environmental Engineering, Concordia University, Montreal, Canada

<sup>b</sup>Institut de recherche Robert-Sauvé en santé et en sécurité du travail, Montreal, Canada

\*Corresponding email: mau\_chav@encs.concordia.ca

## 1. ABSTRACT

The prediction of pollutant dispersion in urban environment is an extremely complex phenomenon, particularly in the vicinity of a cluster of buildings. Dispersion of effluents released from stacks located on building roofs are severely affected by adjacent surroundings. This paper investigates the impact of an upstream building on the near field of a pollutant source in terms of dilution distribution on the roof of an emitting building. The study was carried out using Computational Fluid Dynamics (CFD) approach with Realizable  $k-\epsilon$  for turbulent flow modeling. A limited number of cases were also modelled in a wind tunnel for validation purposes. The study shows that when the source is located within the recirculation zone, dilution is highly sensitive to the height of the upstream building and much less sensitive to the width and length of the upstream building. It is also shown that dilution value has an asymptotic behavior which defines the particular point where dilution becomes independent of the upstream building configuration. Some discrepancies between CFD and wind tunnel data were found, specifically for extreme configurations e.g. significantly taller upstream building. These differences are mainly due to the inherent unsteady fluctuations in the wake of buildings which are not detectable by RANS.

## 2. INTRODUCTION

Air quality in urban areas has gained increasing interest in recent years due to its significant influence in human health. In 2004, Health Canada estimated that air pollution caused nearly 6000 premature deaths each year in 8 cities in Canada (Judek et al., 2004). The Canadian Medical Association extended this study and estimated that approximately 21000 deaths could be attributed to air pollution in 2008 in the entire country. The air pollution has a wide range of effects, with

36 chronic respiratory diseases and loss of life the most serious; however this problem carries also  
37 high economical damage including lost productivity, life quality degradation and health care costs,  
38 which have been estimated to \$8 billion (CMA, 2008).

39  
40 In the built environment increasing exhaust emissions from institutional, industrial buildings and  
41 vehicular traffic are inevitable. Toxic and odorous emissions affecting the urban environment and  
42 degrading human health are present in every city. One of the most common urban pollution phe-  
43 nomenon is associated with contaminants released from rooftop stacks. Depending on the average  
44 airflow, the turbulence of flow and the building-generated turbulence, pollutants can be trapped in  
45 recirculation zones and affect sensitive areas as, for example, fresh air intakes. This closed circuit  
46 path is known as re-ingestion of pollutants.

47  
48 In a dense urban area there is plenty of opportunity for re-ingestion and the health impact of this  
49 episodic pollution event is a cause for concern for health physicists and regulatory agencies. Un-  
50 fortunately, the state of art is not sufficiently advanced to allow building engineers to apply appro-  
51 priate design criteria to avoid this problem for new construction or to help alleviate the re-ingestion  
52 of pollutants for existing buildings. Consequently, incidents involving poor air quality continue to  
53 be recorded and documented.

54  
55 Complexities in airflow and pollutant transport due to terrain conditions, local topography and  
56 buildings make it very difficult to assess plume concentrations (Saathoff et al., 2009). This study  
57 will focus on the effect of an upstream building on dispersion in the immediate vicinity of the  
58 source of pollutant. Four different upstream configurations have been tested in the Boundary Layer  
59 Wind Tunnel of Concordia University, Canada and compared with earlier results for an isolated  
60 building case. In particular, the impact of plume dilutions on the change in height, along wind and  
61 across wind dimensions of the upstream building were studied. In the past, studies performed by  
62 Wilson et al. (1998) and Stathopoulos et al. (2008) showed that the presence of a taller upstream  
63 building produces higher concentrations on the rooftop of the emitting building. Currently,  
64 ASHRAE (2007) gives guidelines for determining plume dilutions for an isolated building, i.e.  
65 without considering the effects of adjacent buildings and local turbulence. Studies performed by  
66 Hajra et al. (2010) have shown that ASHRAE (2007) predicts rather unrealistic and overly con-  
67 servative dilutions. More recently, Computational Fluid Dynamics (CFD) has been a useful tool  
68 in assessing plume dilutions in the built environment. However, CFD simulations require valida-  
69 tions with field and wind tunnel measurements.

70  
71  
72  
73  
74  
75  
76  
77  
78  
79  
80  
81  
82  
83  
84  
85  
86  
87  
88  
89  
90  
91  
92  
93  
94  
95  
96  
97  
98  
99  
100  
101  
102

This paper presents wind tunnel data for tracer gas released from a rooftop stack in the presence of upstream buildings for stack height of 0.005 m (full scale equivalent to 1 m) at exhaust momentum ratio  $M$ , defined as the ratio between the exhaust velocity ( $V_e$ ) and wind velocity at the building height ( $U_{B1}$ ), equal to 1. The spacing between the buildings was fixed to 0.1 m (20 m) and the stack location was 0.1 m (20 m) from the upwind edge of the emitting building. Results are compared to CFD simulations using the Realizable  $k-l$  model (Shih et al., 1995) for different turbulent Schmidt numbers ( $Sc_t$ ) and dilution from ASHRAE (2007).

### 3. WIND TUNNEL SETUP

The wind tunnel experiments were carried out in the open circuit of the Building Aerodynamics boundary layer wind tunnel Laboratory at Concordia University, Montreal, Canada. The wind tunnel is 1.8 m by 1.8 m in cross-section and 12.2 m in length. The buildings tested in the wind tunnel were made of timber on a 1:200 scale. According to Snyder (1981) while modeling non-buoyant plume exhaust, certain criteria should be satisfied:

- Geometric similarity
- Building Reynolds Number  $> 11000$
- Stack Reynolds Number  $> 2000$
- Similarity of wind tunnel flow with that in atmospheric surface layer
- Equivalent stack momentum ratio.

Tracer gas consisting of a mixture of Sulphur hexafluoride ( $SF_6$ ) and Nitrogen was released from a roof stack of an emitting building named B1. A multi-syringe pump was used to collect the gas samples to determine the concentration of effluents at various receptors with a sampling time of 1 minute. A Gas Chromatograph (GC) was used to assess the gas concentrations that were collected using syringe samplers. The velocity at building height was measured to be 6.2 m/s in the wind tunnel. The buildings were considered to be in an urban terrain with a power law exponent of 0.31 (Simiu and Scanlan, 1996). Additional details on the experimental conditions used in this study are described in Stathopoulos et al. (2008).

103 The pollutant dispersion was evaluated in terms of normalized dilution following the formulation  
104 suggested by Wilson (1979):

105

$$106 \quad D_{\text{Normalized}} = (D_r Q) / (U_{B1} H_{B1}^2) \quad (1)$$

107

108 where  $D_r = C_e / C_r$  is the dimensionless concentration coefficient at the coordinate location (re-  
109 ceptor),  $C_e$  = contaminant mass fraction in exhaust (ppm),  $C_r$  = contaminant mass fraction at the  
110 coordinate location (ppm),  $Q$  is the flow rate at the exhaust ( $\text{m}^3/\text{s}$ ),  $H_{B1}$  is the height of the emitting  
111 building called B1 ( $H_{B1} = 0.075\text{m}$ ), and  $U_{B1}$  the wind speed at  $H_{B1}$  ( $U_{B1} = 6.2 \text{ m/s}$ ). The ratio at the  
112 stack outflow is  $M = V_e / U_{B1}$  (where  $V_e$  is the exhaust velocity).

113

114 Figure 1 shows the emitting building B1 receptor locations. Dilution concentration measurements  
115 were carried out using receptors (4 upwind and 6 downwind the stack) located centrally on the  
116 rooftop of B1 and spaced 0.025m apart and 0.125m from lateral edges. Receptors were located on  
117 rooftop primarily due to the plume trajectory in the presence of an upstream building, as discussed  
118 further in Wilson et al. (1998), and for direct comparisons with the ASHRAE (2007) dispersion  
119 model.

120

### 121 **Figure 1**

122

123 Five building models were used to generate four different upstream configurations. The dimen-  
124 sions of each building used in the study are provided in Table 1 with a generic schema of config-  
125 urations shown in Figure 2.

126

### 127 **Table 1**

128

129 The following configurations were simulated in the wind tunnel

130

131 - Configuration 1: B1 (Isolated building)

132 - Configuration 2: B2 upstream of B1

133 - Configuration 3: B3 upstream of B1

134 - Configuration 4: B4 upstream of B1

135 - Configuration 5: B5 upstream of B1

136

137 **Figure 2**

138

## 139 4. NUMERICAL SIMULATION

140

### 141 4.1 Computational model and boundary conditions

142

143 CFD is a useful tool for simulation of turbulent flow and pollutant dispersion around buildings.

144 The present work was carried out using the commercial software FLUENT based on the Reynolds-

145 Averaged Navier-Stokes equations (RANS). The effects of different turbulence models have been

146 tested in previous flow field around bluff bodies (Yap, 1987; Launder and Kato, 1993; Tsuchiya et al.,

147 1997, Tomigana and Stathopoulos, 2009); however a clear statement about the optimum choice of

148 turbulence model for flow around buildings is still not available. The reason is because turbulence

149 models performance depends on the particular case. This paper uses the Realizable  $k-\varepsilon$  turbulence

150 model based on a literature review carried out by the authors in a previous work (Chavez et al.

151 2011). All the transport equations (momentum, energy,  $k$ ,  $\varepsilon$  and concentration) were discretized

152 using a second-order upwind scheme. Pressure interpolation was of second order. The SIMPLE

153 algorithm was used for pressure-velocity coupling.

154

155 Based on recommendations proposed in COST Action (Franke et al., 2007), the dimensions of the

156 computational domain were specified as follows: considering  $H$  as the height of the taller building

157 in the model, the lateral and the top boundary was located  $5H$  away from the building and the

158 outlet boundary was  $20H$  downwind from the building to allow flow development. For the inlet a

159 distance of  $3H$  was adopted in order to minimize the development of streamwise gradients, as

160 discussed in Blocken et al. (2007).

161

162 The numerical model was constructed principally using structured hexahedra grids since it has

163 been proved that this mesh style provides the best computational results (Hefny and Ooka, 2009).

164 In order to reduce the mesh size and considering that all the physical simulations were performed

165 for a unique wind flow (perpendicular to the building face) a symmetry boundary condition was

166 applied at half width of the emitting building, in consequence all calculations correspond to half

167 domain only, see Figure 2. This consideration was verified by comparison with a full domain sim-

168 ulation. Due to the circular section of the stack, an unstructured wedge grid was used in its vicinity.

169 The grid size used in the current work is based on a grid sensitivity analysis performed by the

170 authors in a previous work (Chavez et al., 2011) since dimensions of models and characteristics of

171 pollutants emission remain very similar. In the current work the number of cells was approxi-  
172 mately 600,000 to 800,000 depending on the configuration. The grid resolution was 0.001 m at the  
173 stack and 0.005 m at the edges of the emitting building and increased gradually to 0.0346 m at the  
174 limit of domain.

175  
176 The bottom surface (i.e ground) is specified as a rigid plane with an aerodynamic roughness length  
177  $y_o=0.0033$  m corresponding to  $y_o=0.66$  m in full scale. In FLUENT this roughness length is im-  
178 plemented by the sand-grain roughness height  $k_s$  (m), defined using the function developed by  
179 Blocken et al. (2007):  $k_s=9.793y_o/C_s$ , where  $C_s$  is a roughness constant. Considering the default  
180 value of  $C_s$  equal to 0.5,  $k_s$  should be specified as 0.0646. However, this value is limited to the  
181 distance  $z_p$  of the centroid of the first cell to the bottom domain (in this case  $z_p=0.00187$  m), as  
182 imposed by FLUENT. The effect of this limitation is translated to stream wise changes in the inlet  
183 vertical profile, which attempts to improve the accuracy of CFD simulations. This issue has been  
184 discussed in previous works (Hargreaves and Wright, 2007; Norris and Richards, 2010; Parente et  
185 al., 2011a, 2011b). To reduce the effect of undesired inlet profile, the current study has adopted  
186 the minimization of upstream domain length criterion by specifying  $3H$  (as mentioned previously)  
187 as suggested by Blocken et al. (2007). This option is reasonable in the present case considering  
188 that the wind flow impinging the plume is more affected by the presence of the upstream building  
189 than the roughness length.

190  
191 The approaching mean velocity and turbulence intensity profiles measured in the wind tunnel and  
192 used to specify the inlet boundary layer at the CFD model are shown in Figure 3. Similar to the  
193 experiment, a power law exponent of 0.31 corresponding to urban terrain was used for the study.  
194 The velocity at the building B1 height ( $H=0.075$  m) was  $U_{B1}=6.2$ m/s. The turbulent kinetic energy  
195 profile ( $k$ ) was calculated using  $k=0.5(I_U U)^2$  and turbulent intensity values ( $I_U$ ) measured in the  
196 current wind tunnel experiments. The dissipation rate profile ( $\varepsilon$ ) was defined as  $\varepsilon=u^{*3}/\kappa y$  where  $\kappa$   
197 is the von Karman constant (0.42) and  $u^*$  is the friction velocity obtained from the equation  
198  $u(y)/u^*=1/\kappa(\ln(y/y_o))$  with roughness length  $y_o=0.0033$ m. Top and sides of the domain were mod-  
199 elled as slip walls (zero shear slip). At the outlet an outflow (zero gradient) condition was specified,  
200 to generate a fully developed flow. For walls, the standard wall function was applied because  $y^*$   
201 was between 30 and 300 in a large number of cells. A symmetry boundary condition was added at  
202 half of the emitting building, as explained previously. The pollutant released from stack was sim-  
203 ulated with  $SF_6$  for a particular exhaust momentum ratio  $M=V_e/U_{B1}=1$  (where  $V_e$  is the exhaust  
204 velocity).

205

206 **Figure 3**

207

208 Turbulent Schmidt number ( $Sc_t$ ) is necessary to solve the transport mass equation in CFD predic-  
209 tion of dispersion with RANS and is defined as the ratio of turbulent momentum diffusivity (eddy  
210 viscosity) to the turbulent mass diffusivity ( $Sc_t = \nu_t / D_t$ ). In FLUENT  $Sc_t$  must be declared as input  
211 prior to any calculation or else the default value assumed is 0.7. Past studies have shown the de-  
212 pendence of  $Sc_t$  on simulation of pollutant dispersion from isolated buildings (Tominaga and  
213 Stathopoulos, 2007; Chavez et al., 2011) and hence the present work pays special attention to  $Sc_t$   
214 values

215

## 216 5. RESULTS AND DISCUSSION

217

218 A qualitative comparison between experimental and numerical simulations for dilution on the roof  
219 of the emitting building is presented. Several configurations were evaluated and a single wind  
220 tunnel measurement for each case was used to make a comparison with CFD. The confidence (or  
221 repeatability) of this single measurement was assumed to be within 10%, as it was found by Statho-  
222 poulos et al. (1999) where the same wind tunnel with similar flow characteristics was used. Quan-  
223 titative analysis for every comparison as the quantitative metric proposed by Oberkampff and Bar-  
224 one (2006) has not been used in the presented study.

225

### 226 5.1. Isolated building

227

228 Figure 4 shows the dilution comparison between wind tunnel measurements, CFD for  $Sc_t=0.3$ , 0.7  
229 and ASHRAE (2007). The wind tunnel data correspond to measurements performed in July 2009  
230 (Chavez et al., 2011). The dilution values upstream the stack were too high to be detected by the  
231 chromatograph used in the tests, so data to be compared with CFD are not available. Concerning  
232 the dilution comparison between CFD and experimental data, it is clearly demonstrated that RANS  
233 underestimates dilution when using standard values of  $Sc_t$  ( $Sc_t=0.7$ ) for an isolated building case.  
234 This observation was also pointed out in previous studies (Tominaga and Stathopoulos, 2007;  
235 Chavez et al., 2011). The reason is mainly due to the weakness of RANS to modeling turbulent  
236 diffusion in zones with flow separation, as is the case on the roof of an isolated building. To cali-  
237 brate this underestimation a correct parametrization of turbulent fluxes via the  $Sc_t$  is required

238 (Gousseau et al., 2011). Modification of  $Sc_t$  will influence the spread of pollutant deficiently pre-  
239 dicted by RANS. In this case, dilution calculated by CFD can have acceptable agreement with  
240 experimental values by using  $Sc_t=0.3$ . It is also observed that dilution model proposed by  
241 ASHRAE (2007) predicts very low dilutions, yielding very conservative results.

242

#### 243 **Figure 4**

244

#### 245 5.2. Effect of upstream building height

246

247 The effect of height of a building placed upstream of B1 is presented in Figures 5, 6, 7 and 8.  
248 Figures 5 and 6 show streamlines and normalized dilution field on the middle vertical and hori-  
249 zontal planes at the stack height ( $y = 0.08\text{m}$ ) for Config-3 and Config-5. The height of the upstream  
250 building was changed keeping its width (0.25 m) and length (0.075 m) constant. The spacing be-  
251 tween buildings was also kept constant at 0.1 m. Figure 5 shows an extended wake zone with  
252 secondary vortices behind the two buildings in the vertical and horizontal plane of Config-3. The  
253 vertical plane near the stack shows a combination of upwind and downwind flow. The horizontal  
254 velocity plan shows the important cross flow from the side. The dilution contours reveal that part  
255 of the pollutants are dragged upwind toward the leeward wall of the upstream building. In conse-  
256 quence, a very long dilution distribution along the middle axis was observed downwind the stack.

257

#### 258 **Figure 5**

259

260 Figure 6 shows the vertical and horizontal velocity field and the corresponding dilution contours  
261 for Config-5 (a taller upstream building). Clearly the wake zone was larger than the previous case  
262 and a strong horizontal vortex (not observed previously) near the roof of the upstream building  
263 appears within the recirculation zone. A well-formed vortex between the two buildings is formed  
264 with a diameter equal to the distance between the two buildings. The general pattern of flow reveals  
265 that the wake is characterized by a predominant horizontal upwind velocity component. The cor-  
266 responding dilution contours show that practically the entire plume is trapped and dragged toward  
267 the leeward of the upstream building. When the pollutants reach the leeward wall, they are imme-  
268 diately transported downstream by the sides following the large horseshoe developed around the  
269 buildings.

270

#### 271 **Figure 6**



272

273 Figures 7 and 8 show the influence of upstream building height on the velocity profile immediately  
274 above the stack and the dilution distribution on the roof of B1. The relative height of the upstream  
275 building is identified using the parameter "h" which is the ratio of the upstream building and B1  
276 height ( $h = H_{\text{upstream}}/H_{B1}$ ). Figure 7 shows the along wind velocity component ( $U_x$ ) profile on a  
277 vertical line above the stack. As the height of the upstream building increases, the along wind  
278 component velocity tends to move in the upwind direction. The local velocities near and above the  
279 stack in Config-5 show that the entire flow in this zone is directed upwind. On the other hand, it is  
280 observed that in the same zone the entire flow is directed downstream in the same zone for the  
281 isolated building case.. The range of maximum velocities are near 3 m/s upwind for Config-5 and  
282 9 m/s downwind for the isolated building. For configurations in between these two, the wind pro-  
283 file has a combination of components upwind and downwind. As noted in Figure 8, the dilution  
284 field is affected by these different local velocities in the wake, especially downstream the stack. In  
285 this zone dilution increases as the upstream building height increases following an asymptotic  
286 behaviour. This observation suggests that a change of the upstream building height does not affect  
287 the dilution downwind the stack after a specific "h" starting near 2.8. On the other hand, dilution  
288 distribution upwind the stack seems to be independent of the upstream building height when a  
289 critical height,  $h_c$ , between 1.33 and 1.7, is reached. For values below  $h_c$ , and up to  $h = 1$ , the  
290 dilution distribution upwind the stack is extremely dependant on the upstream building height. It  
291 can thus be concluded that dilution is very sensitive to the height of upstream buildings in areas  
292 downstream the stack, upstream the stack dilution seems to be independent of the upstream build-  
293 ing height for values starting from  $h_c$ . Experimental and numerical results presented a similar trend,  
294 which was characterized by low dilution upwind and high dilution downwind the stack. However,  
295 significant quantitative inconsistencies were registered specially for a much taller upstream build-  
296 ing (Config-5). This is probably due to the inherent fluctuations in the wake of buildings which  
297 are not detectable by RANS. These fluctuations are characterized by unsteady vortical structures  
298 which interact with each other and with the surroundings playing a fundamental roll in the transport  
299 mechanism of pollutants. In consequence, steady RANS will reproduce unrealistic dilution values  
300 in regions where mixing is caused by the advection of generated eddies into the wake. ASHRAE  
301 (2007) predicted very low dilutions, yielding very conservative results.

302

303 **Figure 7**

304

305 **Figure 8**

306

### 307 5.3. Effect of upstream building width and length

308

309 Figures 9 and 10 show the effect of varying width, which is the across wind dimension, of the  
310 upstream building; whereas Figures 11 and 12 show the effect of varying length of the upstream  
311 building. In general, the effect of these two geometric variables produce somewhat similar behav-  
312 ior with that discussed previously for the building height effect. This is low dilution upwind the  
313 stack which is independent to the shape of the upstream building following by dilution that in-  
314 creases along the wind axis for the downwind stack region. The dilution downwind the stack is  
315 different depending on the shape of the upstream building, however it should be noticed that the  
316 effect is relatively less important for both width and length in comparison with the height effect.

317

318 Figures 9 and 10 show the effect of upstream building width in the along wind velocity component  
319 ( $U_x$ ). The relative width of the upstream building is identified using the parameter "w" which is  
320 the ratio of the upstream building width and B1 width ( $w = W_{\text{upstream}}/W_{B1}$ ). The velocity profile  
321 showed a lightly variation for different upstream building width. The corresponding dilution val-  
322 ues upwind the stack are almost independent of the upstream building width and has a relatively  
323 small influence on dilution downstream the stack. For a larger w value, dilution increases mono-  
324 tonically downwind the stack. This is probably because a larger recirculation vortex on side of B1  
325 may be carrying extra fresh air for dilution. It is also noted that for small upstream building widths,  
326 dilution tends to behave as in the case of an isolated building.

327

328 **Figure 9**

329

330 **Figure 10**

331

332 Figures 11 and 12 show the effects of upstream building length. As with previous cases, "l" rep-  
333 resents the ratio of the upstream building length and B1 length ( $l = L_{\text{upstream}}/L_{B1}$ ). As in previous  
334 cases, dilution upwind the stack is almost independent of the upstream building length and dilution  
335 downwind the stack increases when the length of the upstream building decrease. This could be  
336 explained again by the added side recirculation produced by a thin building.

337

338 **Figure 11**

339

340 **Figure 12**

341

342 **6. CONCLUSION**

343

344 The influence of three variables (height, width and length) of an upstream building on pollutant  
345 dispersion in the built environment was examined using wind tunnel experiments and CFD mod-  
346 eling. The dilution of pollutants is affected significantly by the height of the upstream building  
347 especially for the region downwind the stack where a direct dependence on the upstream building  
348 height was observed. In contrast, dilution shows very little sensibility to all configurations for a  
349 region upwind the stack. It is also confirmed that ASHRAE (2007) is too conservative for all cases.  
350 CFD simulations show discrepancies on dilution values downwind the stack for an upstream high-  
351 rise building producing high dilution compared with the wind tunnel. These differences may be  
352 explained by the inaccuracy of steady state RANS to capture dispersion in areas of high turbulent  
353 flow.

354

355

356 **REFERENCES**

357

358 ASHRAE, 2007. Building air intake and exhaust design. ASHRAE Applications Handbook, Chapter 44, American  
359 Society of Heating, Refrigerating and Air-Conditioning Engineering Inc., Atlanta, USA.

360 Blocken, B., Stathopoulos, T., Carmeliet, J., 2007. CFD simulation of the atmospheric boundary layer: wall function  
361 problems. *Atmos. Environ.* 41, 238-252.

362 Canadian Medical Association. No breathing room. National illness costs of air pollution. Ottawa, ON: Canadian

363 Medical Association; 2008. Available from: [www.cma.ca/multi-media/CMA/Content/Images/Inside\\_cma/Of-  
364 fice\\_Public\\_Health/ICAP/CMA\\_ICAP\\_sum\\_e.pdf](http://www.cma.ca/multi-media/CMA/Content/Images/Inside_cma/Office_Public_Health/ICAP/CMA_ICAP_sum_e.pdf). Accessed 2011 Jun 13.

365 Chavez, M., Hajra, B., Stathopoulos, T., Bahloul, A., 2011. Near-field pollutant dispersion in the built environment  
366 by CFD and wind tunnel simulations. *J. Wind Eng. Ind. Aerodyn.* 99 (4), 330-339.

367 Franke, J., Hellsten, A., Schunzen, H., Carissimo, B., 2007. Best practice guideline for the CFD simulation of flows  
368 in the urban environment. Cost Action 732, Quality assurance and improvement of microscale meteorological mod-  
369 els.

370 Gousseau, P., Blocken, B., Van Heijst G.J.F. 2011. CFD simulation of pollutant dispersion around isolated buildings:

371 On the role of convective and turbulent mass fluxes in the prediction accuracy. *J. Hazard. Mater.* 194, 422-434.

372 Hajra, B., Stathopoulos, T., Bahloul, A., 2010. Assessment of pollutant dispersion from rooftop stacks: ASHRAE,  
373 ADMS and wind tunnel simulation. *Build. Environ.* 45, 2768-2777.

374 Hargreaves, D., Wright, N., 2007. On the use of the  $k-\varepsilon$  model in commercial CFD software to model the neutral  
375 atmospheric boundary layer. *J. Wind Eng. Ind. Aerodyn.* 95, 355-369.

376 Hefny, M., Ooka, R., 2009. CFD analysis of pollutant dispersion around buildings: effect of cell geometry. *Build.*  
377 *Environ.* 44(8), 1699-1706.

378 Judek, S., Jessiman, B., Stieb, D., Vet, R., 2004. Estimated number of excess deaths in Canada due to air pollution.  
379 Ottawa, ON: Health Canada; Available from: [www.metrovancouver.org/about/publications/Publications/AirPollutionDeaths.pdf](http://www.metrovancouver.org/about/publications/Publications/AirPollutionDeaths.pdf). Accessed 2011 Jun 13.

381 Launder, B.E., Kato, M., 1993. Modeling flow-induced oscillations in turbulent flow around a square cylinder. In  
382 ASME Fluid Engineering Conference.

383 Norris, S.E., Richards, P.J., 2010. Appropriate boundary conditions for computational wind engineering models re-  
384 visited. In: *Proceedings of the Fifth International Symposium on Computational Wind Engineering (CWE2010)*  
385 Chapel Hill, North Carolina, USA, May 23-27, 1-8.

386 Oberkampf, W. L., & Barone, M. F. 2006. Measures of agreement between computation and experiment: Validation  
387 metrics. *J. Comp. Phys.*, 217(1), 5-36.

388 Parente, A., Gorié, C., van Beeck, J., Benocci, C., 2011a. Improved  $k-\varepsilon$  model and wall function formulation for the  
389 RANS simulation of ABL flows. *J. Wind Eng. Ind. Aerodyn.* 99, 267-278.

390 Parente, A., Gorié, C., van Beeck, J., Benocci, C., 2011b. A Comprehensive modelling approach for the neutral at-  
391 mospheric boundary layer: Consistent inflow conditions, wall function and turbulence model. *Boundary-Layer Me-*  
392 *teorol.* 140, 411-428.

393 Saathoff, P., Gupta, A., Stathopoulos, T., Lazure, L., 2009. Contamination of fresh air intakes due to downwash  
394 from a rooftop structure. *J. Air Waste Manage. Assoc.* 59, 343-353.

395 Stathopoulos T., Lazure L. and Saathoff P. 1999. Tracer gas reingestion of Building Exhaust in an Urban Environ-  
396 ment, IRSST research report R-213 Institut de recherche Robert-Sauvé en santé et en sécurité du travail, Montreal,  
397 Canada.

398 Shih, T.H., Liou, W.W., Shabbir, A., Yang, Z., Zhu, J., 1995. A new  $k-\varepsilon$ - eddy-viscosity model for high Reynolds  
399 number turbulent flows. *Comp. Fluids.* 24(3), 227-238.

400 Simiu, E., Scanlan, R. H., 1996. *Wind effects on structures: fundamentals and applications to design.* 3rd Edition,  
401 Wiley Interscience Publication, USA.

402 Snyder, W. H., 1981. Guidelines for fluid modelling of atmospheric diffusion. EPA office of Air quality, planning  
403 and standards, Research Triangle Park, USA, EPA-600/8-81-009.

404 Stathopoulos, T., Hajra, B., Bahloul, A., 2008. Analytical evaluation of dispersion of exhaust from rooftop stacks on  
405 buildings. IRSST research report R-576, *Institut de recherche Robert-Sauvé en santé et en sécurité du travail*, Mon-  
406 treal, Canada.

407 Tominaga, Y., Stathopoulos, T., 2007. Turbulent Schmidt numbers for CFD analysis with various types of flowfield.  
408 Atmos. Environ. 41, 8091-8099.

409 Tominaga, Y., Stathopoulos, T., 2009. Numerical simulation of dispersion around an isolated cubic building: com-  
410 parison of various types of  $k-\epsilon$  models. Atmos. Environ, 43, 3200-3210.

411 Tsuchiya, M., Murakami, S., Mochida, A., Kondo, K., Ishida, Y., 1997. Development of a new  $k-\epsilon$  model for flow  
412 and pressure fields around bluff body. J. Wind Eng. Ind. Aerodyn. 67&68, 169-182.

413 Wilson, D.J. 1979. Flow patterns over a flat roofed buildings and application to exhaust stack design.  
414 ASHRAE Transactions, 85(2), 284-295.

415 Wilson, D. J., Fabris, I, Ackerman M Y., 1998. Measuring adjacent effects on laboratory exhaust stack design.  
416 ASHRAE Transactions, 88 (1), 513-533.

417 Yap, C.J., 1987. Turbulent Heat and Momentum Transfer in Recirculating and Impinging Flows. PhD thesis, Uni-  
418 versity of Manchester.

419

420  
421  
422  
423  
424  
425  
426  
427  
428  
429  
430  
431  
432  
433  
434  
435  
436  
437  
438  
439  
440  
441  
442  
443  
444  
445  
446  
447  
448  
449  
450  
451  
452  
453  
454  
455  
456  
457  
458  
459  
460  
461  
462  
463  
464  
465  
466  
467  
468  
469  
470  
471  
472  
473  
474  
475

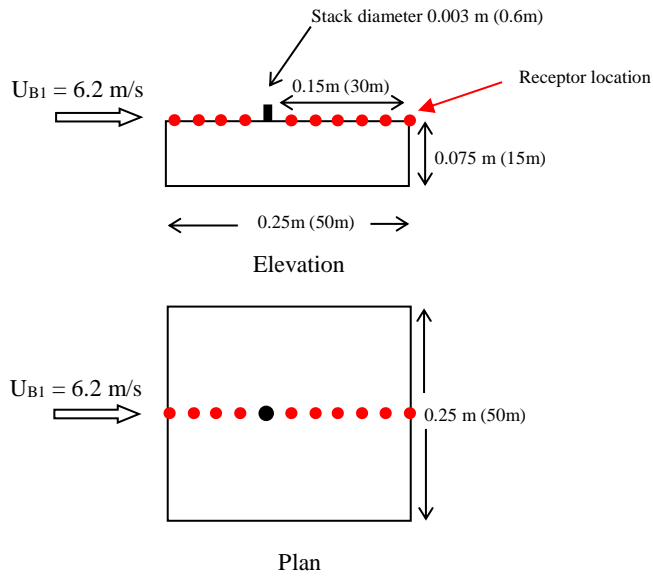


**Figure 1: Elevation and plan view of the emitting building, B1 (wind tunnel model).**

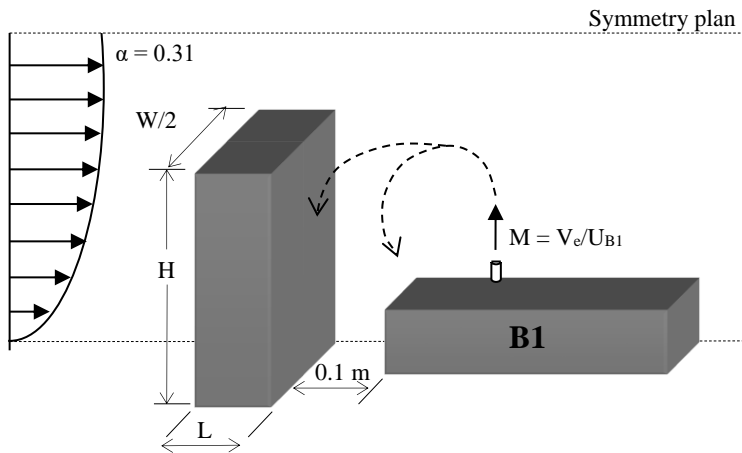


**Figure 2: Isometric view of B1 with an upstream building (CFD model)**

476  
477  
478  
479  
480  
481  
482  
483  
484  
485  
486  
487  
488  
489  
490  
491  
492  
493  
494  
495  
496  
497  
498  
499  
500  
501  
502  
503  
504  
505

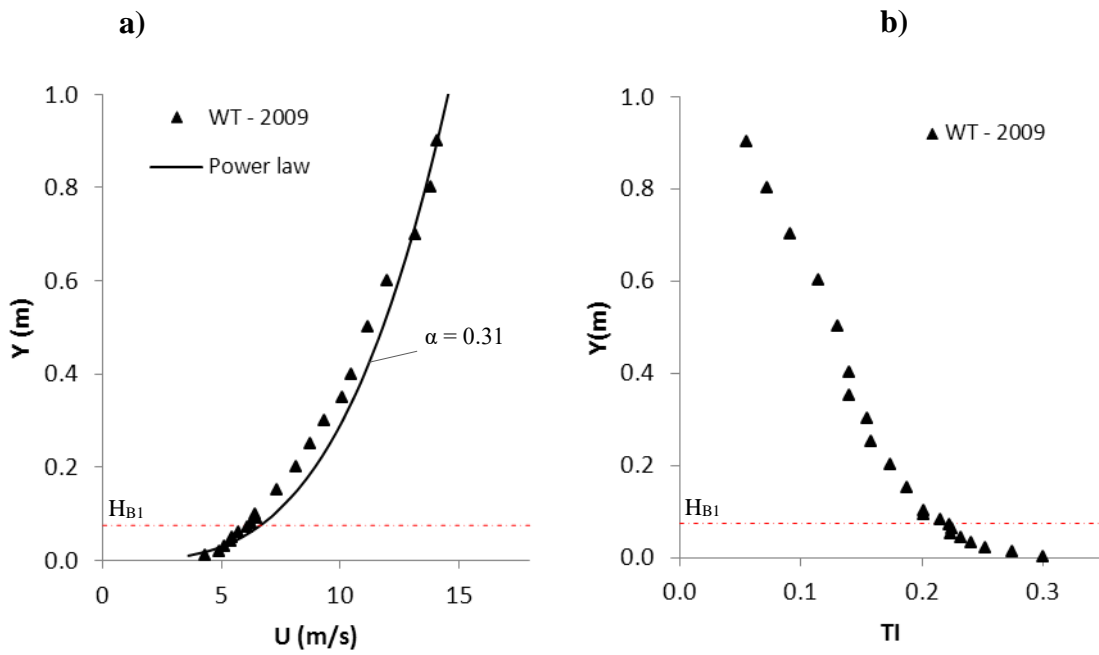


**Figure 3: Inlet profile measurements from wind tunnel. a) Velocity profile b) Turbulence intensity.**

506  
507  
508  
509  
510  
511  
512  
513  
514  
515  
516  
517  
518  
519  
520  
521  
522  
523  
524  
525  
526  
527  
528  
529  
530  
531  
532  
533  
534  
535  
536  
537  
538  
539  
540  
541  
542  
543  
544  
545  
546  
547  
548  
549  
550  
551  
552  
553  
554  
555  
556  
557  
558  
559  
560  
561  
562  
563  
564  
565  
566

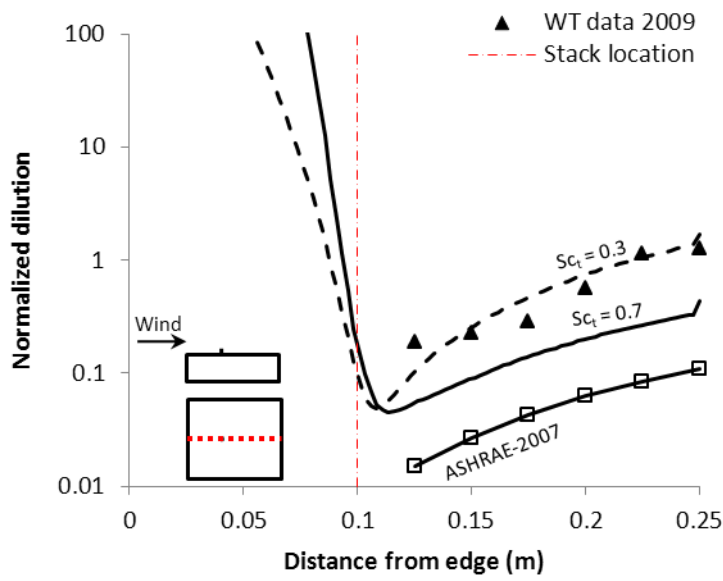
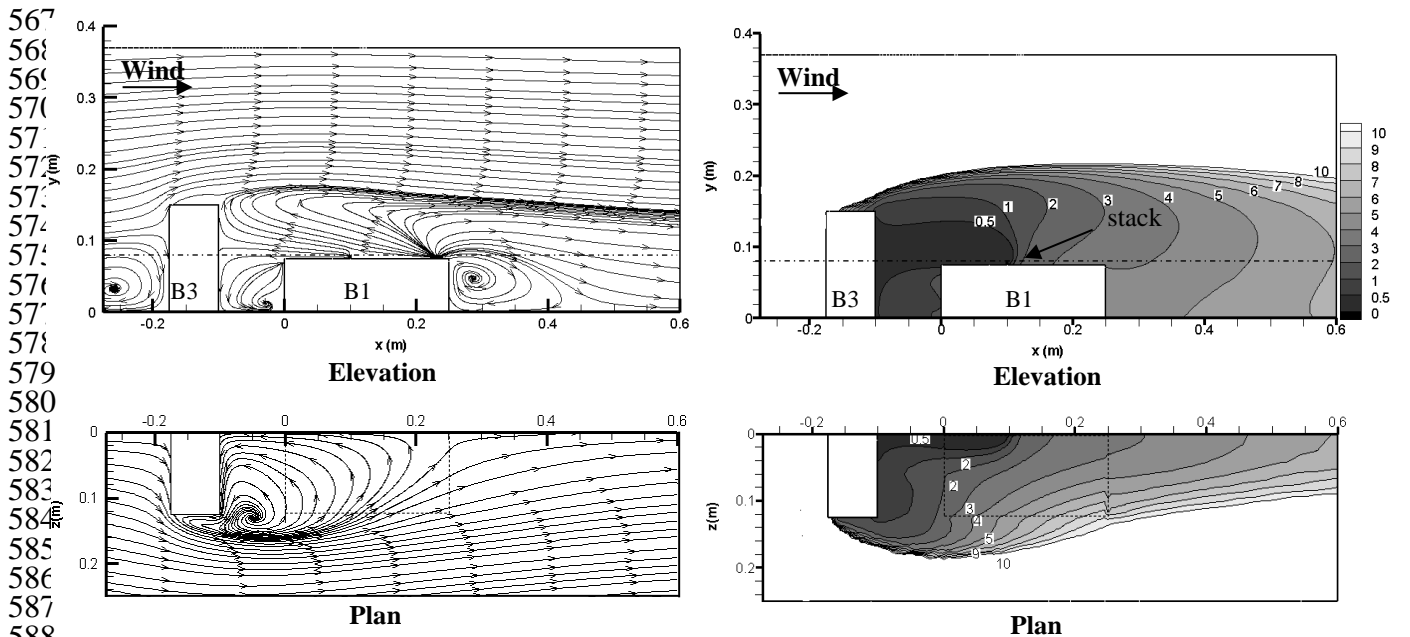
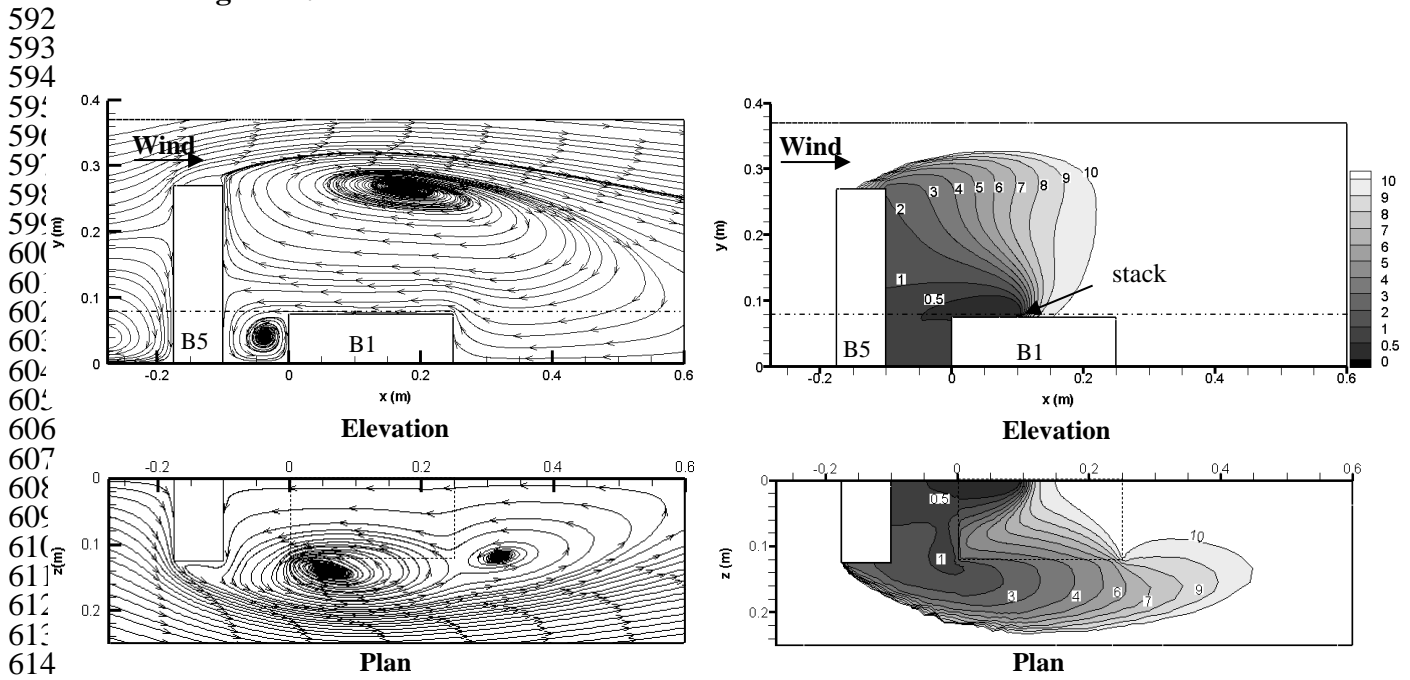


Figure 4. Normalized dilution on isolated building roof, B1, for different  $Sc_t$ . a) 2009 Wind tunnel data and CFD-Realizable  $k-\epsilon$ .





590 **Figure 5. Elevation and half plan view (at  $H = 0.08$  m) of streamlines and dilution contours**  
 591 **of Config-3.  $Sc_t = 0.7$ . Dilution scale from 0-10.**



616 **Figure 6. Elevation and half plan view (at  $H = 0.08$  m) of streamlines and dilution contours**  
 617 **of Config-5.  $Sc_t = 0.7$ . Dilution scale from 0-10.**

618  
619  
620  
621

622  
 623  
 624  
 625  
 626  
 627  
 628  
 629  
 630  
 631  
 632  
 633  
 634  
 635  
 636  
 637  
 638  
 639  
 640  
 641  
 642  
 643  
 644  
 645  
 646  
 647  
 648  
 649  
 650  
 651  
 652  
 653  
 654  
 655  
 656  
 657  
 658  
 659  
 660  
 661  
 662  
 663  
 664  
 665  
 666  
 667  
 668  
 669  
 670  
 671  
 672  
 673  
 674  
 675  
 676  
 677  
 678  
 679  
 680  
 681  
 682

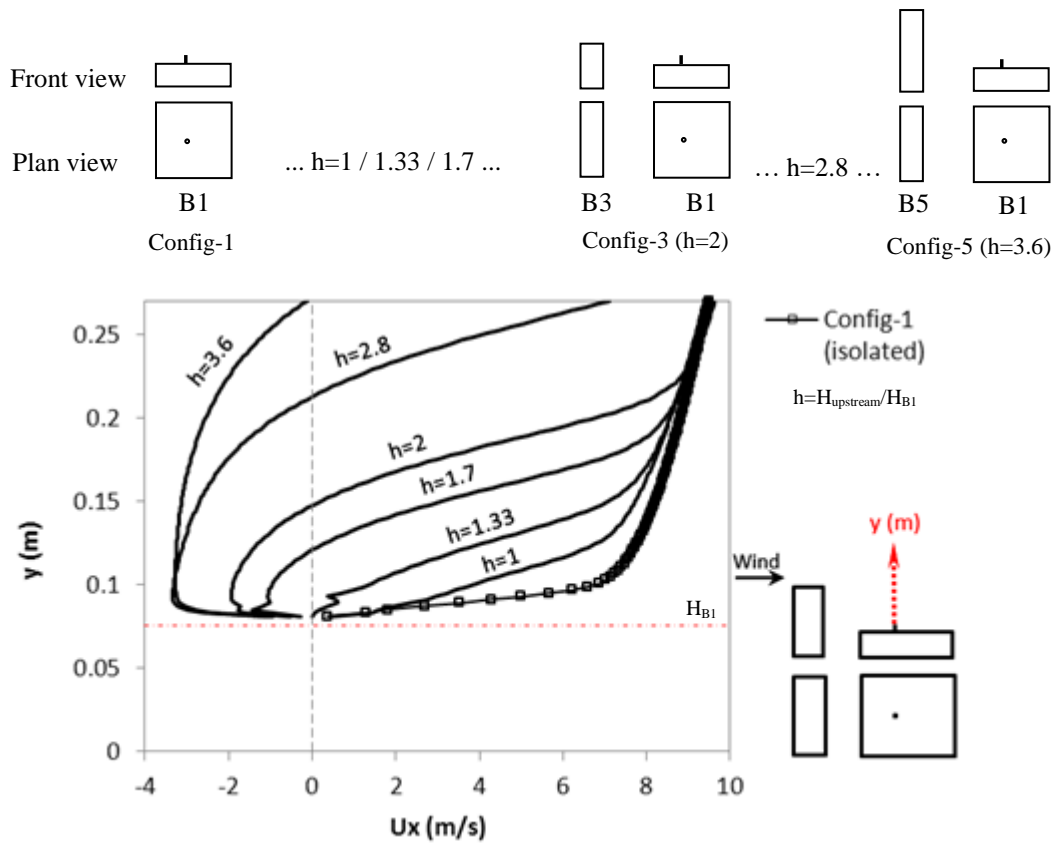


Figure 7. Velocity profile,  $U_x$  (m/s) along the indicated plotting line. Effect of upstream building height, using Realizable  $k-\epsilon$  turbulence model with  $Sc_t = 0.7$ .

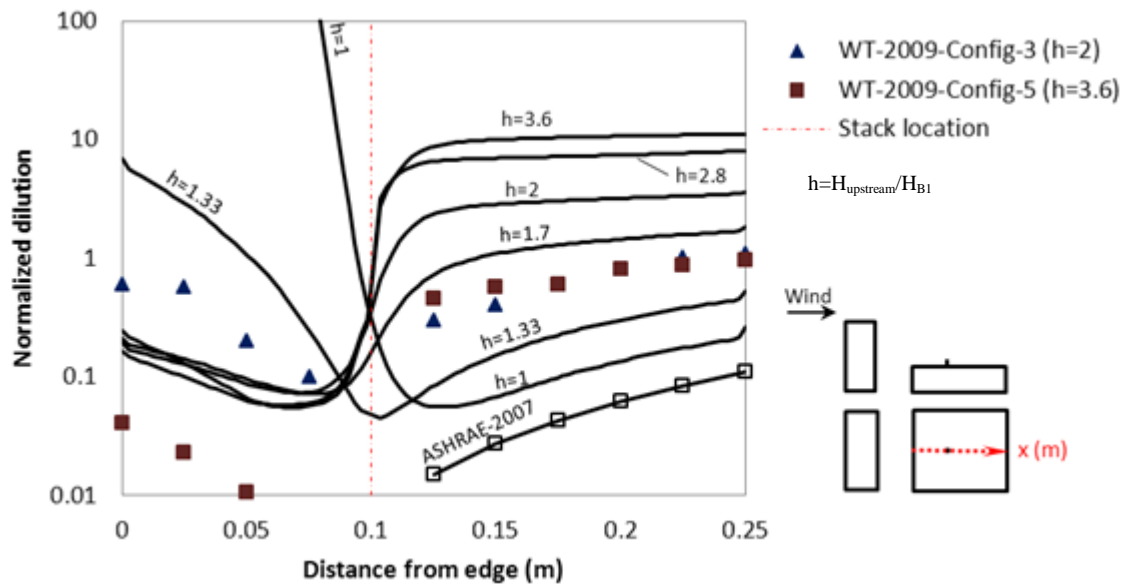
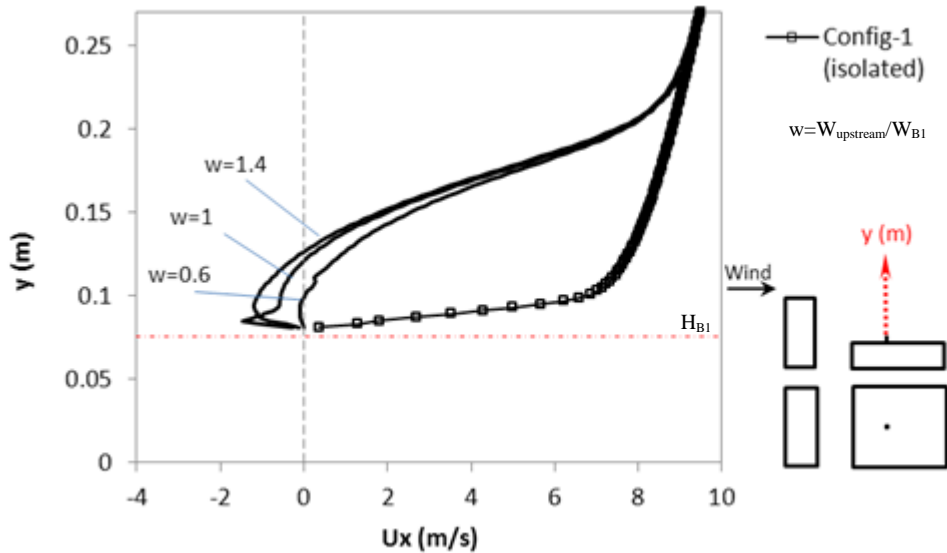
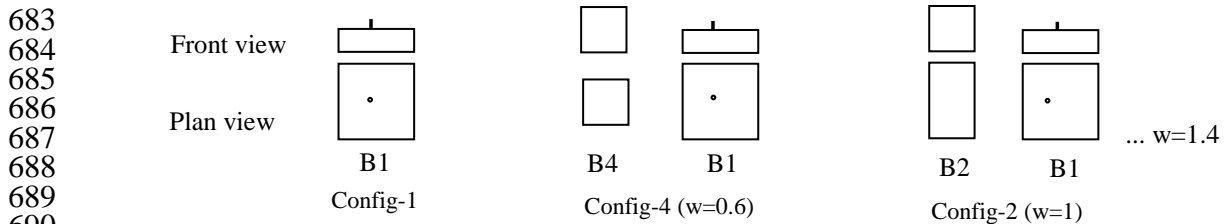
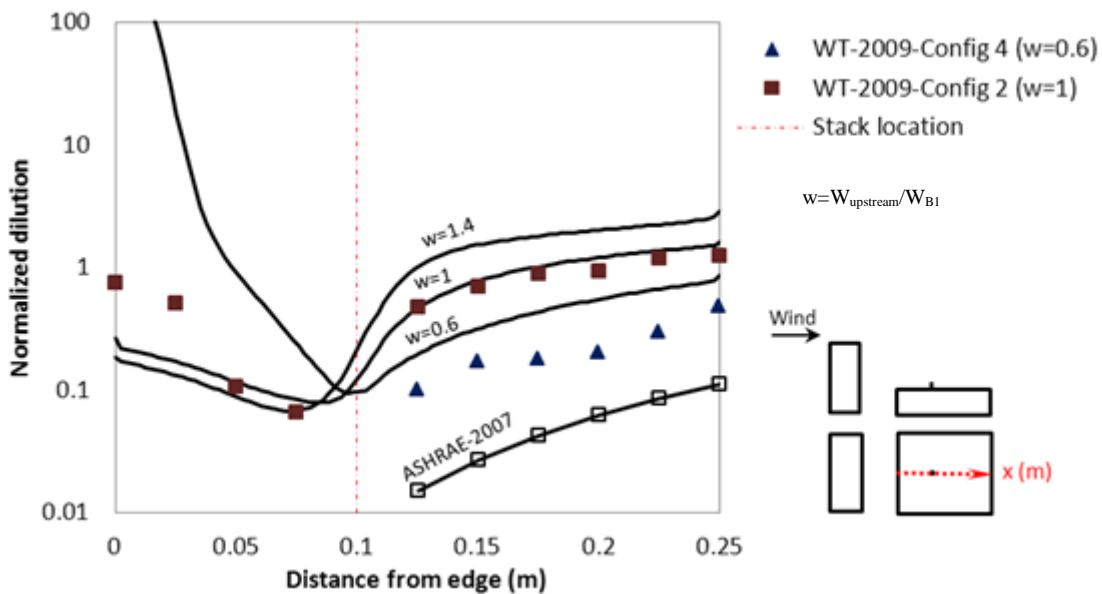


Figure 8. Effect of upstream building height on dilution on the roof of B1. All cases consider stack height = 0.005 (m) and  $M = 1$  (exhaust momentum).



712  
713  
714

**Figure 9. Velocity profile,  $U_x$  (m/s) along the indicated plotting line. Effect of upstream building width, using Realizable  $k-\epsilon$  turbulence model with  $Sc_t = 0.7$**



741  
742  
743  
744

**Figure 10. Effect of upstream building width on dilution on the roof of B1. All cases consider stack height = 0.005 (m) and  $M = 1$  (exhaust momentum).**

745  
746  
747  
748  
749  
750  
751  
752  
753  
754  
755  
756  
757  
758  
759  
760  
761  
762  
763  
764  
765  
766  
767  
768  
769  
770  
771  
772  
773  
774  
775  
776  
777  
778  
779  
780  
781  
782  
783  
784  
785  
786  
787  
788  
789  
790  
791  
792  
793  
794  
795  
796  
797  
798  
799  
800  
801  
802  
803  
804  
805

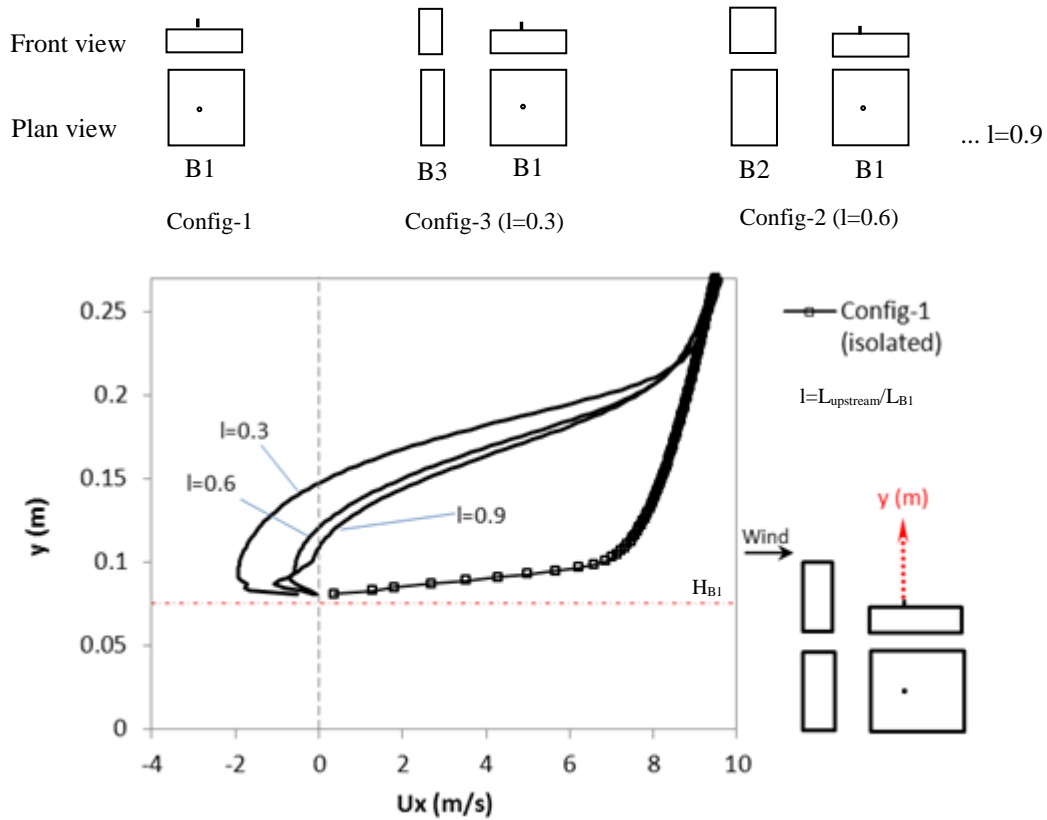


Figure 11. Velocity profile,  $U_x$  (m/s) along the indicated plotting line. Effect of upstream building length, using Realizable  $k-\epsilon$  turbulence model with  $Sc_t = 0.7$ .

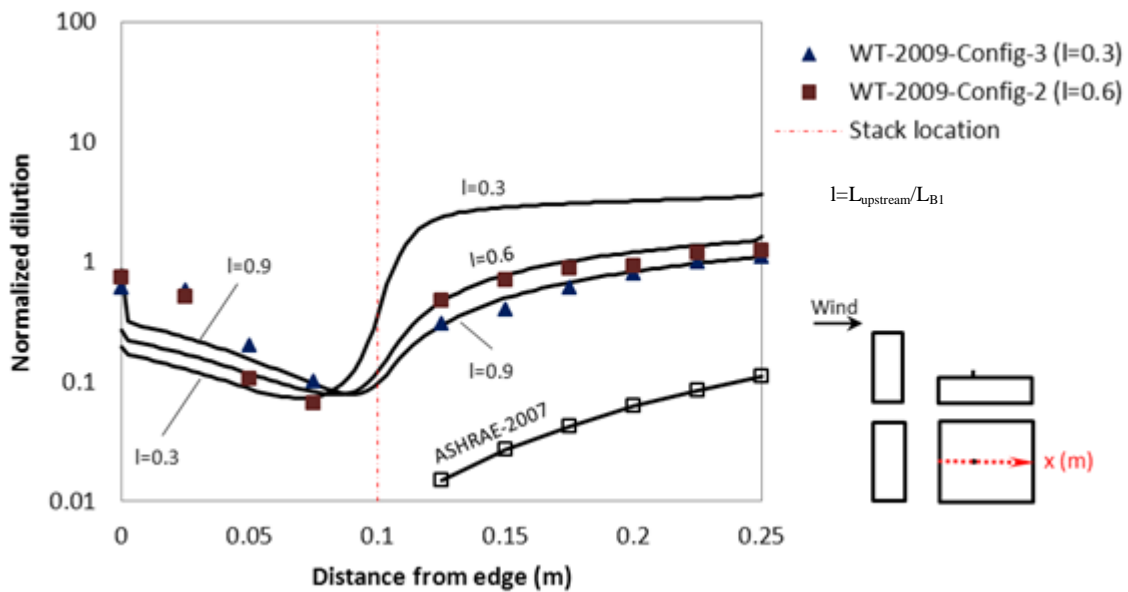


Figure 12. Effect of upstream building length on dilution on the roof of B1. All cases consider stack height = 0.005 (m) and  $M = 1$  (exhaust momentum).

806 **Table 1. Building models for CFD and wind tunnel experiments**  
807

Building	Height, H (m)	Width , W (m)	Length, L (m)
B1 (emitting building)	0.075 (15)	0.25 (50)	0.25 (50)
B2	0.15 (30)	0.25 (50)	0.15 (30)
B3	0.15 (30)	0.25 (50)	0.075 (15)
B4	0.15 (30)	0.15 (30)	0.15 (30)
B5	0.27 (54)	0.25 (50)	0.075 (15)

808 NB: Width refers to across wind dimension

809

810

811